Feature Article:
DOI. No. 10.1109/MAES.2018.170145

UAV System for Photovoltaic Plant Inspection

***Pia Addabbo, Antonio Angrisano, Mario Luca Bernardi,* Giustino Fortunato University, Benevento, Italy**
***Graziano Gagliarde, Alberto Mennella,* TopView S.r.l., Caserta, Italy**
***Marco Nisi,* Sistematica S.p.a., Terni, Italy**
***Silvia Liberata Ullo*, University of Sannio, Benevento, Italy**

INTRODUCTION

In the last two decades, growing attention on climate issues has caused the worldwide increase of Photovoltaic (PV) plant production and installation, and the consequent promotion of clean energy policies, with large amounts of incentives and funding made available in the specific sector by Governments and the European Economic Community itself. Increasing PV distribution and installation has to ask for efficient and low-cost methods for inspection to monitor functionality and guarantee performance. A big concern of PV plant owners is to rely on efficient maintenance procedures. Recognizing degradation and defects of PV cells is a very important issue to allow immediate intervention and substitution of modules to avoid output power losses and performance degradation.

New systems, based on the use of Unmanned Aerial Vehicles (UAVs), have been thought to substitute human workers inspecting the PV plants to reduce maintenance costs and intervention times. In recent years, extended research has been conducted on automated remotely controlled systems for PV fields inspection, realized through the employment of UAVs to substitute human intervention on the PVs and to reduce human activity of data collection and postprocessing [1]. UAVs allow realizing the detection of defects in PV plants thanks to the fusion of computer vision algorithms and high accuracy Global Navigation Satellite System (GNSS) positioning techniques. Particularly, the use of UAVs in PV plants monitoring together with the GNSS positioning techniques allows getting reliable information for the diagnosis of PV systems being able to detect and tag anomalies on the defective panel. The advantages of UAVs employment are several: low costs, automated detection, large area coverage, accuracy in defect detection through the combination of different sensors, and cameras [2].

Furthermore, information acquired by UAVs can be transmitted to a remote console where subsequent interventions can be activated by the detected anomalies. Maintenance companies equipped with suitable tools can in this way conduct an a priori analysis of the PV plant, which can be then compared with an a posteriori PV plant performance evaluation based on the final energy produced.

As already underlined above, within the employment of UAVs for PV plant monitoring, a big step forward has been represented by the incorporation of GNSS information to solve problems related to accurate panel positioning and geo-referencing over the PV plant. In this field of investigation, a low-cost GNSS Real Time Kinematic (RTK) receiver has been proposed to be mounted on board the UAV system for locating the defective cells [3], [4].

The goal of the authors of this article is to describe some critical aspects of direct geo-referencing, image acquisition, panel recognition, and faulty module detection in the specific case of PV plant inspection. Besides this, they will present interesting results come out of a validation campaign performed taking into account different datasets.

THE REMOTELY PILOTED AIRCRAFT SYSTEM (RPAS)

The model of proposed system architecture is represented in Figure 1, where a UAV performs a mission flying over a PV field to collect optical and thermal images of solar panels. The data gathered by the UAV are processed through a computer vision algorithm running on-board the vehicle in tight synergy with a geo-software module, capable of tagging thermographic images using fixed centimeter-level positions provided by the commercial U-blox M8 series receivers. The accurate positioning provided by GNSS signals enables the automation of the entire process allowing to correctly geo-referencing the defective panel inspected by the thermal camera on-board the UAV. Finally, this information is provided to the remote service center in charge of the defect identification and PV plant management. We refer to the overall architecture as Easy-PV Remotely Piloted Aircraft System (RPAS) Architecture, since the work presented

Authors' current addresses: P. Addabbo, A. Angrisano, M. L. Bernardi, Giustino Fortunato University, Viale Raffaele Delcogliano, 12, Benevento (BN), 82100, Italy; G. Gagliarde, A. Mennella, TopView S.r.l., Via Alessandro Pertini, 25D, San Nicola La Strada, 81020 (CE), Italy; M. Nisi, Sistematica S.p.a., Via Bramante, 43, 05100, Terni (TR), Italy; Silvia Liberata Ullo, University of Sannio, Piazza Roma 21, Benevento, (BN) 82100 Italy, E-mail: (p.addabbo@unifortunato.eu).
Manuscript received July 21, 2017, revised October 10, 2017, and ready for publication November 17, 2017.
Review handled by W. Walsh.
0885/8985/18/$26.00 © 2018 IEEE

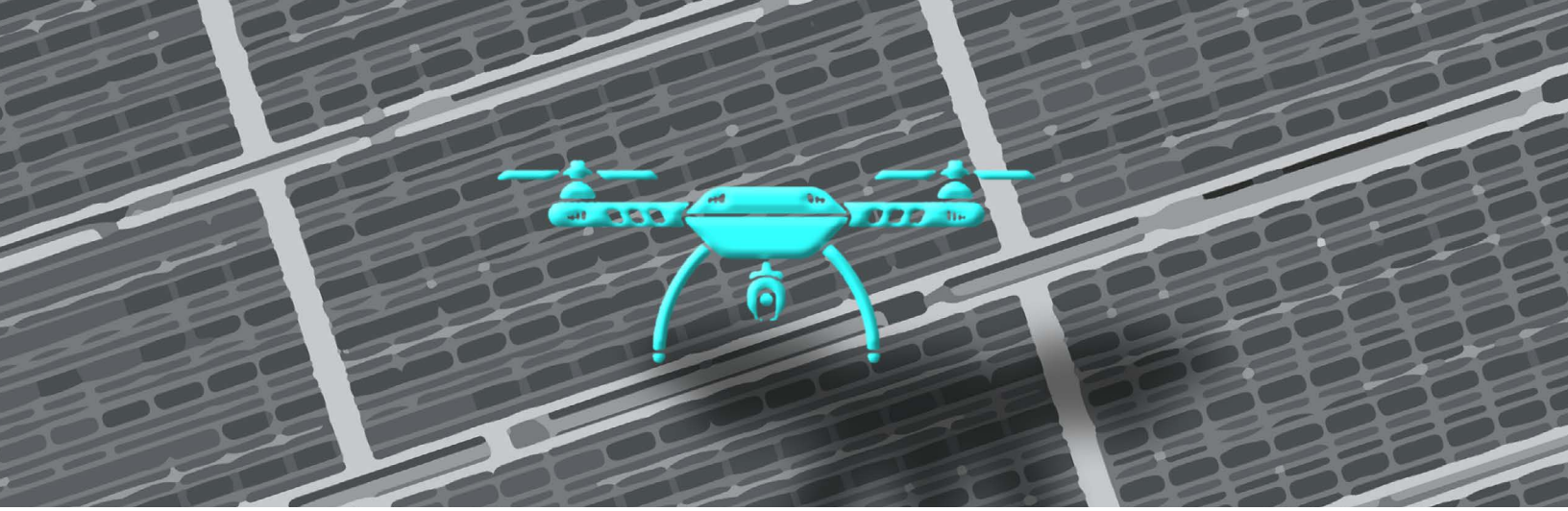

in this article is part of the ongoing activities performed in the framework of the EASY-PV project sanctioned under H2020-Galileo-2015-1 call.

THE PAYLOAD DESCRIPTION AND SPECIFICATIONS

In Figure 1, the architecture of the entire Easy-PV RPAS is represented. The payload designed for this specific application consists in:

- a thermal camera;
- an optical camera and a gimbal;
- an On-Board Computer (OBC).

The most important aspect in the payload designing is the realization of the specific InterFace block required to command and control the thermal sensor and all the mechanism necessary to keep the pointing error as low as possible and to keep the device aligned for optimal nadiral acquisition during the RPAS movements. The heart of the payload is represented by the OBC element that has in charge different tasks such as:

- handling sensors acquisitions;
- handling commands for payload control from pilot or payload operator;
- storing thermal and optical acquired images;
- hosting and handling computer vision algorithm;
- hosting and handling the GEO-Tagging SW module;
- managing acquired data towards the Service Center.

In Figure 2, a block diagram of the implemented payload is highlighted. The blue blocks represent the hardware modules of the payload; the yellow blocks represent the main software components.

The acquired optical and thermal images are geo-tagged with a precise position information obtained from the GNSS C94-M8P U-blox receiver. The position (referred to the center of the antenna) is shifted into the thermal camera optical center. Such information is used by the OBC element to tag each image center with accurate geographical references.

Moreover, the computer vision block has embedded PV panel shape recognition features, while the typologies of thermal anomalies are handled as plug in. Such information is available to the pilot (or payload operator) as screen overlay in real time to add additional remarks to each panel (identified or not) in the case of need. For instance, in the case of bad identification of PV panels or the case of false positives from the algorithm, the pilot (or payload operator) may flag suspect panels during flight operations through his remote control screen. Such information is useful in after-flight post-processing to allow

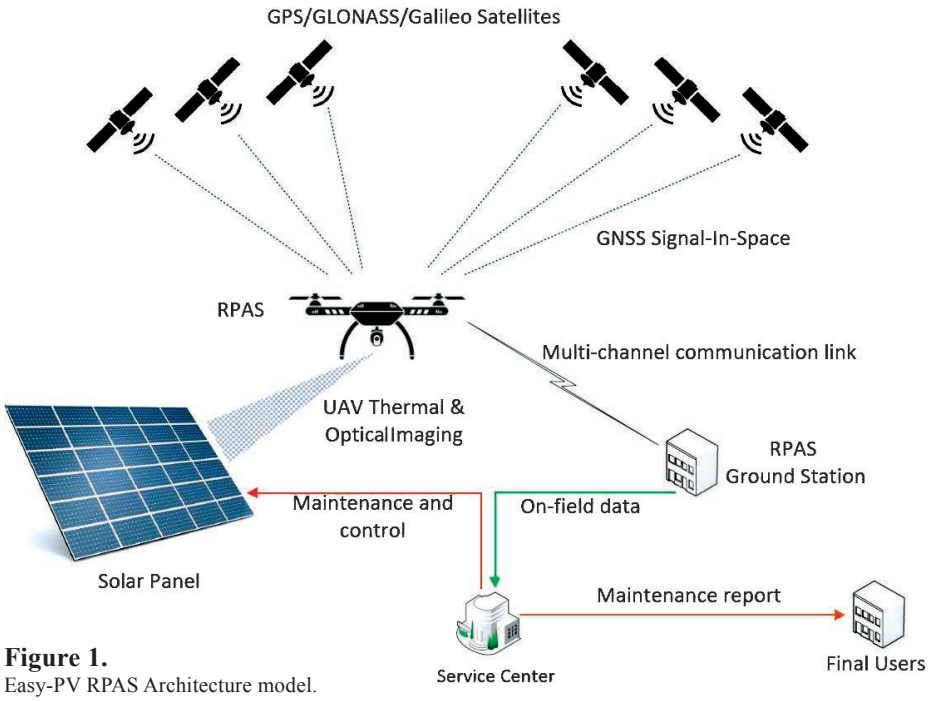

Figure 1.
Easy-PV RPAS Architecture model.

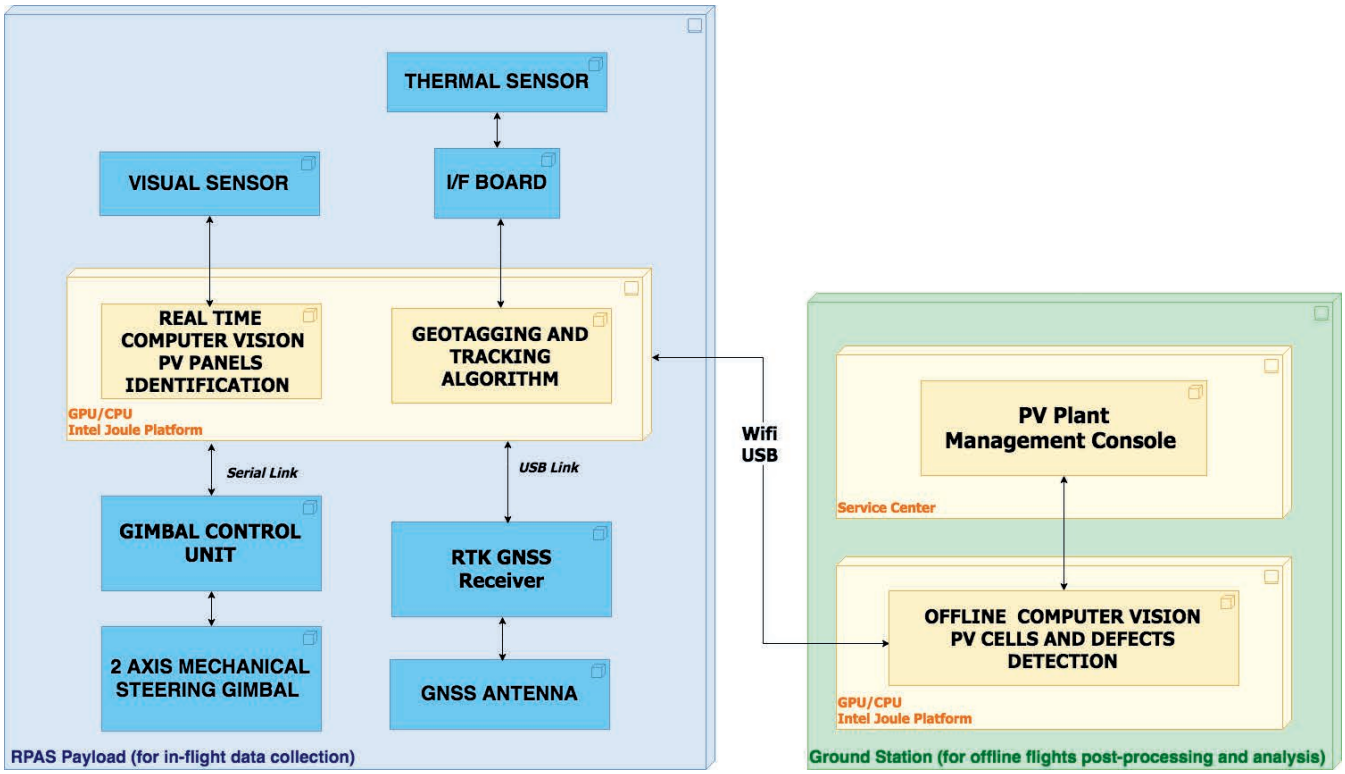

Figure 2.
RPAS Payload block diagram.

the second (offline) part of the algorithm to refine on the flagged thermographies before the generation of the final Extensible Markup Language streams to be sent to the Service Center.

GEO-REFERENCING ISSUES

1) GNSSs: Satellite-Based navigation systems able to provide tridimensional position, velocity, and synchronization to Universal Time Coordinated timescale. The GNSS operational principle is based on the trilateration scheme, which consists of determining unknown locations by measuring ranges from or towards known points.

In GNSS context, the trilateration is tridimensional, so the position loci are spheres, centered in the satellite positions, with radii equal to the measured distances between satellites and user/receiver. In ideal conditions, i.e. if the range measurements were accurate, at least three satellites should be available to make possible the three-dimensional positioning.

In real conditions, four GNSS satellites (from a single system) are necessary because a forth unknown must be taken into account, the offset between the receiver clock and the reference timescale. GNSS satellites transmit electromagnetic signals (in the L-band), and the distance satellite–receiver is determined by the elapsed time Δt from the transmission instant of the signal from GNSS satellite to the user reception instant (one-way ranging), multiplied by the signal speed.

Several GNSS systems are currently available. Global Positioning System (GPS) is the most widespread GNSS, managed by the United States Department of Defense and fully operative since 1994. GLObal NAvigation Satellite System (GLONASS) is the Russian alter ego of GPS. It arose in the early 1980s at the same time of GPS. After a crisis period in the nineties, since 2003 it has been submitted to a modernization phase, and currently, it is fully operational, and it has become a valid alternative to GPS. The European Galileo and the Chinese BeiDou are further GNSS systems, and nowadays they are almost completely deployed. All the previously mentioned GNSS systems have the same operational principle, and they are designed to be compatible and interoperable. Their combined use in a multi-constellation approach is very beneficial in a critical environment, an urban canyon or mountainous areas, where a single GNSS might be unable to provide accurate and continuous positioning.

2) Absolute positioning: Absolute or Single Point Positioning (SPP) is the fundamental GNSS operational mode. It involves the use of a single receiver and it is based on the PseudoRange (PR) measurement, which is the measured range between satellite and receiver affected by clock errors and other error sources (such as atmospheric, relativistic, propagation, noise). The PR measurement equation is shown below [5]:

$$\rho = d + cdt_u + cdt_s + \Delta d_o + \Delta d_i + \Delta d_t + \Delta d_{mp} + \Delta d_n + \varepsilon \quad (1)$$

where:

- ρ is the pseudo range measurement, defined as the measured range between receiver and satellite,
- d is geometric distance between receiver and satellite,

- cdt_u and cdt_s are respectively the receiver and satellite clock offsets scaled by the speed of light,
- Δd_o is the orbital error,
- Δd_i and Δd_t are respectively the ionospheric and tropospheric delays,
- Δd_{mp} is the multipath error,
- Δd_n is the error related to receiver noise,
- ε includes the unmodeled errors.

In SPP, the atmospheric errors are reduced using suitable models and the satellite clock offset is corrected using information from the GNSS ground segment, included in the navigation message. The other errors remain uncorrected and would degrade the SPP performance.

Equation (1) is then rearranged, comprising four unknowns, i.e. the three user coordinates (included in the distance) and the receiver clock offset, so at least four pseudo range equations are necessary to estimate the unknowns. Equation (1) is not linear in the unknowns, hence a linearization around a nominal state (consisting of approximate user position and clock offset) is usually performed.

It is worth to notice that the SPP position has an accuracy of about 5–10 meters [6] and so it is unusable in applications with stringent requirements as mapping or precision farming.

3) Relative positioning: A typical approach to overcome SPP shortage, regarding accuracy, is the relative or differential mode, which makes use of one or more reference stations, placed in known surveyed positions around the GNSS receiver with unknown coordinates (at maximum 100 Kilometers). Differential mode, simply called Differential GNSS (DGNSS), is based on the spatial correlation of several measurement error sources, i.e. errors in the reference station measurements are expected to be very similar to those experienced by a nearby user. The pseudorange error sources, cdt_s, Δd_{orb}, Δd_{iono}, Δd_{tropo}, are spatially correlated and in the differential mode they are cancelled or strongly reduced. In open-sky, where drones typically operate, the ionospheric error is the most influencing, so in this scenario the DGNSS is very effective, improving the accuracy to 1–2 meters [6]. To obtain better performance, such as centimeter-level positioning, the carrier-phase measurement should be used along with pseudorange. The most common technique using carrier-phase is Real Time Kinematic (RTK), which exploits the differential concept too.

PR-based DGNSS technique could be implemented in either position or measurement domain. In the first case, at the reference station, it is computed the difference between the estimated and the known position, which is broadcast to the user and applied directly as position correction. This approach is very simple, but it does not consider the possible inconsistencies between the algorithms used by reference and user receivers. For this reason, it is currently adopted when there is no access to user measurements, such as in a cell phone using GPS. In measurement domain, at the reference station, the differences between the measured and the known ranges are computed and are broadcast to the user, which uses them as corrections for pseudoranges. This approach is very common, and it is adopted for several applications as maritime navigation.

The application considered herein, i.e. identification of defective photovoltaic panels by drones equipped with a thermal camera, requires a very accurate kinematic positioning, which currently can be obtained, in GNSS context, only using RTK technique. In this work, the receiver based on RTK has not been available from the beginning for problems of electromagnetic incompatibility with the antenna as built, so a PR-based DGNSS approach has been followed. Moreover, the adopted GNSS device is unable to provide raw data (e.g. pseduorange, carrier-phase, Doppler measurements), and so a position-domain DGNSS, based on National Marine Electronics Association (NMEA) information [7], is implemented. In the proposed algorithm, the only data necessary from the rover are GGA and GSA NMEA messages, while raw data are required from the reference station. GGA NMEA message contains the SPP coordinates of the rover, while GSA message contains the identifiers of the satellites used for the solution.

The measurement corrections, computed at the reference station, are projected on the position domain using the design matrix. In the considered test, a reference station placed at S. Nicola la Strada (Caserta), far few Kilometers from the rover, is used. The reference station belongs to the GNSS Campania Network and can receive both GPS and GLONASS measurements.

THE IMAGE ACQUISITION SYSTEM: PV MODULE IDENTIFICATION AND DEFECT DETECTION

The Image Acquisition procedure is based on a very precise processing system that receives images from the thermal camera in input and produces final outputs through the proposed Computer Vision Algorithm. As already highlighted geo-referencing operations are crucial since precision is the precondition of a correct and satisfactory data processing for the entire system. Thus, it is necessary, at the moment, the utilization of the DGPS technique which improves accuracy of the present receiver, mounting on board the U-blox NEO-M8N. As already mentioned, although the U-blox NEO-M8N measures are less accurate with respect to those of RTK, they introduce a very interesting novelty since initial services of the Galileo constellation, supported by the NEO-M8N GNSS module, have become available only recently. Moreover, as already explained, DGNSS can compensate many of the error sources by highly improving accuracy.

The core of the Image Acquisition System is the Computer Vision Algorithm. It performs both PV module identification and defect detection and gives a unique ID for each panel and a precise relative position of defects in the metadata. Notably, we are interested in finding PV defectiveness and PV failure, defined as an effect that results in safety or power loss for a PV module [8], [9]. The causes of defects in the PV panels can be damages occurred during the planning, the transportation and the installation stages, which could produce, for example, glass breakage, with a consequent loss of PV performance, or effects of adverse environmental impacts. Among the main measurements methods used to identify

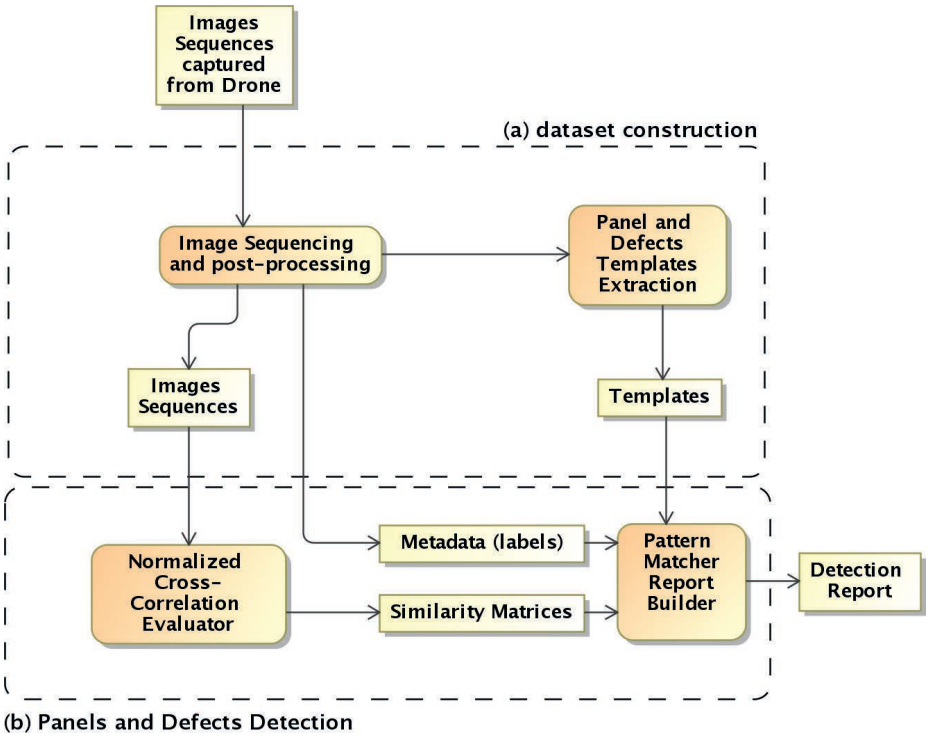

Figure 3.
Flowchart of the Computer Vision algorithm.

PV defects, infrared imaging represents one of the most diffused techniques first of all because it is a noninvasive method for detection of thermal anomalies, and secondly because this technique has reached very high levels of performance in defect detection concerning other methodologies. Infrared imaging is suitable to detect many defects on PV plants, such as faults in bypass diodes, mechanically damaged cells, hot spots, and fault contact points, that represent the main PV plant defect typologies [10]. An example of visible and thermal imaging of the same panels is shown in Figure 4; it is evident the effectiveness of using thermal imaging for defects detection with respect to visible.

In this work, the proposed Computer Vision Algorithm, whose flowchart is shown in Figure 3, is based on the template matching technique, a high-level machine vision procedure for identification of the parts on an image that match a predefined template [11].

The algorithm is implemented using the OpenCV library, an open source project that started in 1999 by the computer-vision community [12], and it uses a Normalized Cross Correlation as a similarity measure for template matching [13].

EXPERIMENTAL SETUP AND RESULTS

As already underlined, the images captured by the onboard thermal camera need an accurate positioning to enable the automation of the entire process allowing to correctly geo-referencing the defective panel. Images have to be tagged using fixed positions provided by the GNSS receiver. At the beginning, the use of an RTK receiver was scheduled for the collection of geo-referenced data. Unfortunately, when employed, it presented electromagnetic interference problems with the devices on board the UAV, due to the magnet which the RTK antenna is provided with. For this reason, it has been ordered a specially customized antenna whose specifications have been properly designed and sent to the manufacturer for its fabrication. Meanwhile, it has been decided to begin data acquisition through the use of the U-blox NEO-M8N GNSS receiver in conjunction with the Differential GNSS mode, as explained previously.

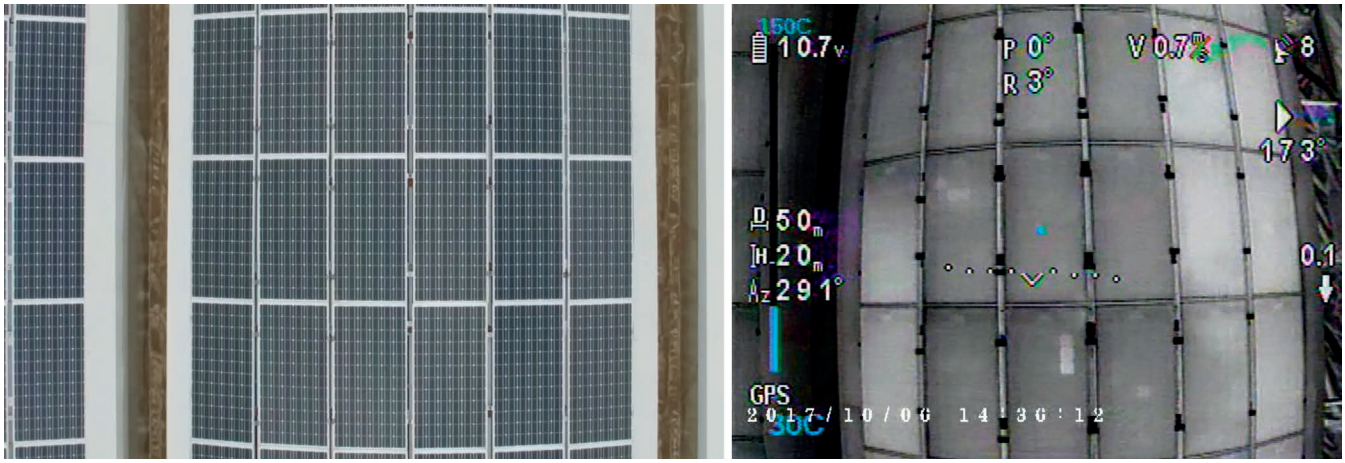

Figure 4.
Example of healthy and broken panels in visible (left) and thermal (right) images (panel defect in light blue).

Figure 5.
DJI Matrice 100 flight platform.

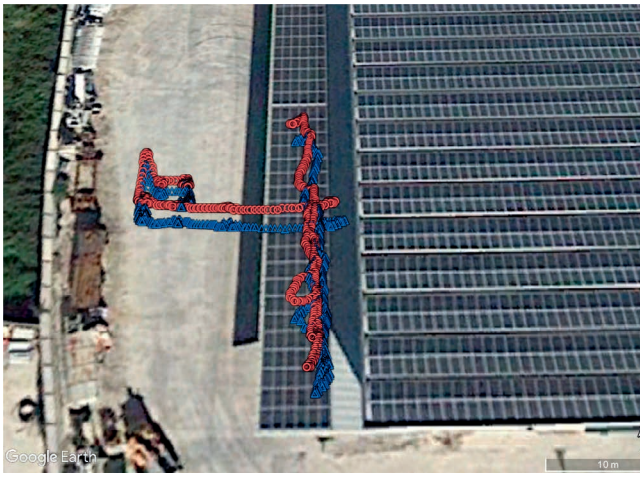

Figure 6.
An example of flight on the area under test with and without differential correction: DGPS (blue triangle), SPP (red circle).

In the considered test, to perform DGNSS, a reference station placed at San Nicola la Strada (Caserta) and far few Kilometers from the rover has been used. The chosen reference station belongs to the GNSS Campania Network, and it can receive both GPS, Galileo, and GLONASS measurements.

The dataset used for this work consists of a series of flights on a test site in Lo Uttaro, a location in the province of Caserta, Italy. The UAV used for testing is shown in Figure 5. It has been done flying over the test site with the manually navigated DJI Matrice 100 flight platform. The UAV has been equipped with the onboard Thermal Camera Flir Vue Pro for thermal images acquisition in the 7.5–13.5 μm spectral band. In Figure 6, it is shown a flight on the area used for the test: the SPP positions extracted from the NMEA file are depicted with red circle while the DGPS positions with blue triangles.

In Figure 7, results of the proposed computer vision algorithm are shown, where a series of six consecutive images are

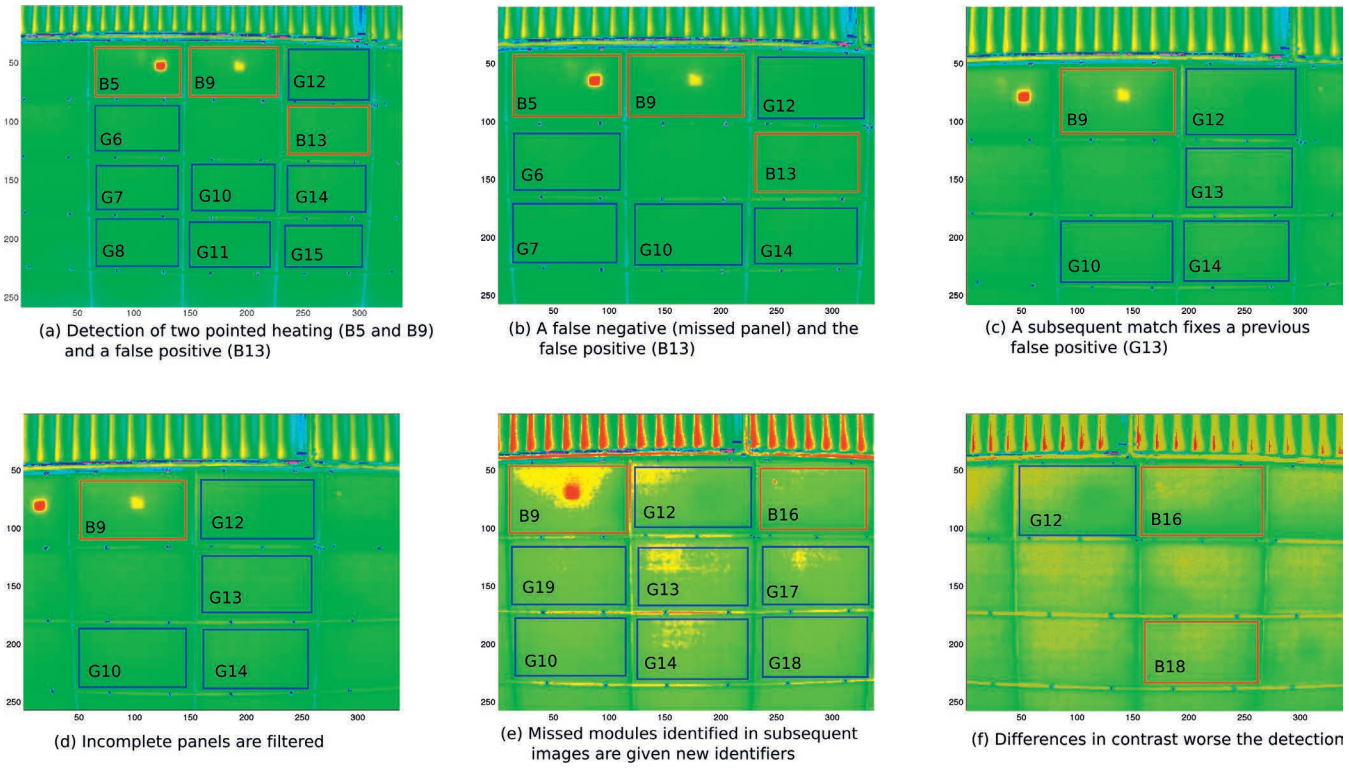

Figure 7.
Panels identification and defect detection: a black box with a G-number ID represents an identified panel while a blue box with a B-number ID is a panel with detected defects.

Table 1.

Precision, Recall and F-Measure Metrics for Panel and Defects Detection, Obtained for Different Thresholds									
Dataset	Threshold	Panel Detection				Defect Detection			
		Precision	Recall	F-Measure	Time (sec)	Precision	Recall	F-Measure	Time (sec)
Sequence 1 (86 images)	0,15	0,10	1,00	0,18		0,00	1,00	0,01	
	0,25	0,13	1,00	0,22		0,01	1,00	0,01	
	0,35	0,17	0,98	0,28		0,01	1,00	0,02	
	0,45	0,25	0,95	0,40		0,02	1,00	0,03	
	0,55	0,40	0,93	0,56	45 s	0,03	1,00	0,06	28 s
	0,65	0,46	0,93	0,61		0,06	1,00	0,11	
	0,75	0,56	0,91	0,69		0,11	1,00	0,19	
	0,85	0,63	0,89	0,74		0,60	0,75	0,67	
Sequence 2 (184 images)	0,95	0,80	0,86	0,83		0,75	0,75	0,75	
	0,15	0,10	1,00	0,18		0,02	1,00	0,05	
	0,25	0,13	1,00	0,22		0,04	1,00	0,09	
	0,35	0,17	0,96	0,28		0,12	0,93	0,21	
	0,45	0,25	0,93	0,39		0,24	0,93	0,38	
	0,55	0,40	0,90	0,55	108 s	0,33	0,90	0,49	55 s
	0,65	0,46	0,86	0,60		0,53	0,87	0,66	
	0,75	0,56	0,84	0,67		0,81	0,87	0,84	
	0,85	0,63	0,82	0,71		0,83	0,83	0,83	
	0,95	0,81	0,79	0,80		0,85	0,77	0,81	

analyzed. Black boxes with a G-number ID are used to identify panels on the PV plant. The panels that are contained in the images are correctly and uniquely identified as shown in the first row of images in Figure 7, while some panels are missing in the other case, shown in the second row of the same Figure. Blue boxes with a B-number ID are used to identify defects on the PV plant panels. Two heating points (IDs: B5 and B9) are correctly detected, even if of different dimensions, and the false positive (ID: B13) present in both (a) and (b), is then corrected in the subsequent shot (c).

Three metrics have been defined and used to evaluate the classification results: Precision, Recall, and F-Measure.

The precision has been computed as the proportion of the examples that truly belong to a specific class among all those which were assigned to that class. It is the ratio of the number of correct items that are detected by the total number of irrelevant and relevant items detected:

$$\text{Precision} = \frac{tp}{tp + fp} \tag{2}$$

where *tp* indicates the number of true positives and *fp* indicates the number of false positives.

The recall has been computed as the proportion of items that were assigned to a specific class, among all the items that truly belong to that class, i.e., how much the class has been covered. It is the ratio of the number of relevant items detected to the total number of relevant items in the search space:

$$\text{Recall} = \frac{tp}{tp + fn} \tag{3}$$

where *fn* indicates the number of false negatives.

The F-Measure is a measure of test accuracy, interpreted as a weighted average of the Precision and the Recall parameters above specified:

$$\text{F-Measure} = 2 \times \frac{Precision \times Recall}{Precision + Recall} \tag{4}$$

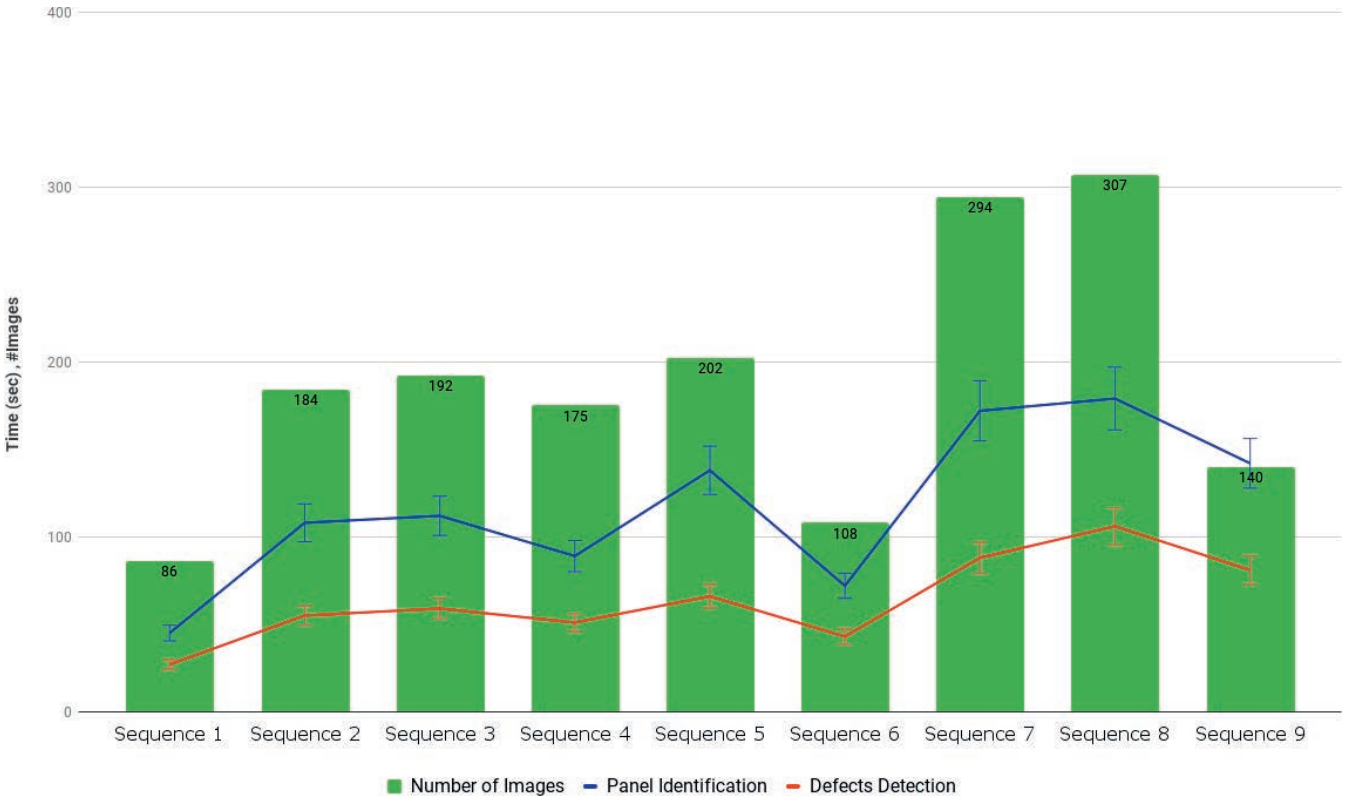

Figure 8.
Detection times for both panel and defects.

We have evaluated the effectiveness of the classification method with the procedure summarized below:

1. build a testing set *T* (gold standard) in which modules are identified and classified by an expert as "Good" or "Bad";
2. apply the classifier to each element of T to detect modules and defects;
3. compare classifier's detection with the gold standard and evaluate performance metrics.

The metrics obtained are shown in Table 1. Time columns represent the average time, expressed in seconds, needed to build the classifier and to perform the detection on two flight sequences. In Figure 8, times are reported for a wider set of sequences of different sizes. The trend confirms that panel identification weighs more than defects detection. The reason of this difference resides in the sizes of templates and the number of passes to perform classification. First of all, templates of panels are larger than the template of defects and this influences cross-correlation computation. Moreover, panel identification requires a two-pass algorithm using two templates, one with defects and one without defects, i.e., a healthy one.

The following consideration can be made:

- the F-measure ranges from 0,18 to 0,83 for panel detection and from 0,01 to 0,75 for defect detection;
- best results for panels and defects detection are obtained for the threshold of respectively 0.96 and 0.985; above these values, F-measure starts to decrease.
- reducing the threshold increases the Recall but quickly lowers the Precision: this can be seen more clearly in Figure 9 that reports Precision and Recall versus the threshold for Panels and Defects detection.

CONCLUSIONS AND FUTURE WORK

In this article, a computer vision approach applied to a PV plant for the identification of the panels and the detection of thermal anomalies has been proposed. The approach integrates geographic information gathered from GNSS with results of a computer vision template matching algorithm applied to thermal images. This combination allows to perform panel identification by assigning to each module an identifier that remains consistent across different flight sessions. Through the proposed matching algorithm different templates have been exploited, to detect both panel extension and the presence of defects. The proposed approach opens up to further work to be focused mainly on the following points, as already discussed in [3]: a barometric altimeter to be tested in order to assess the RPAS altimeter resolution; a UAV/RPAS ground speed of less than 3 m/s; a gimbal orientation normal to object reference system; the evaluation of the misalignments (few milliseconds) introduced by wind gusts; assessment of the PV panels in the case of lack of information about PV panels placement in a planar surface; inclination of the PV panels that reduces their cross-section as seen from the UAV/RPAS; introduction of sensor lens distortion that has to be assessed and mitigated during the tests, since it accounts

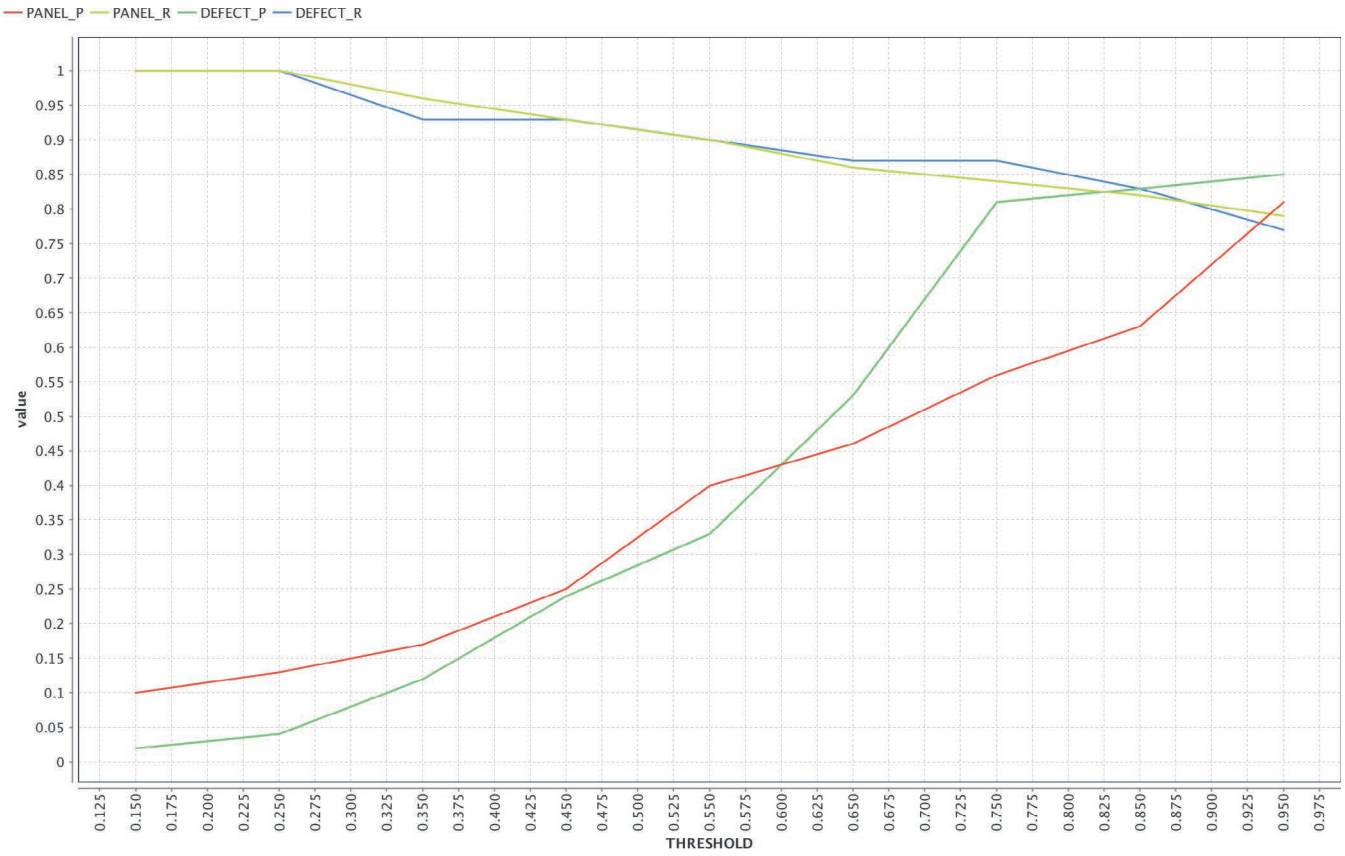

Figure 9.
Precision and recall versus threshold for panels and defects detection.

for one of the most significant error source budget; error in position resolution obtained from the rover on-board of GNSS receiver. ◈

ACKNOWLEDGMENT

The work presented in this article is a part of the ongoing activities performed in the framework of EASY-PV project sanctioned under H2020-Galileo-2015-1 call for Small and Medium Enterprise (SME) based EGNSS application having grant agreement number 687409. The project started off on Feb. 01, 2016 and shall end on Jan. 31, 2018. The project is coordinated by Sistematica S.p.A with contributions from other partners, namely, Aalborg University, TopView srl, DeepBlue, Entec, and Alpha consultants.

REFERENCES

[1] Grimaccia, F., Leva, S., Dolara, A., and Aghaei, M. Survey on PV modules' common faults after an O&M flight extensive campaign over different plants in Italy. *IEEE Journal of Photovoltaics*, Vol. 7, 3 (May 2017), 810–816.

[2] Grimaccia, F., Aghaei, M., Mussetta, M., Leva, S., and Quater, P. B. Planning for PV plant performance monitoring by means of unmanned aerial systems (UAS). *International Journal of Energy and Environmental Engineering*, Vol. 6, 1 (Mar. 2015), 47–54.

[3] Nisi, M., Menichetti, F., Muhammad, B., Prasad, R., Cianca, E., Mennella, A., et al. EGNSS high accuracy system improving photovoltaic plant maintenance using RPAS integrated with low-cost RTK receiver. In *Proceedings of Global Wireless Summit Conference,* Nov. 2016.

[4] Addabbo, P., Angrisano, A., Bernardi, M., Gagliarde, G., Mennella, A., Nisi, M., et al. A UAV infrared measurement approach for defect detection in photovoltaic plants. In *Proceedings of 2017 IEEE Metrology for Aerospace* (MetroAero Space), Jun. 2017.

[5] Hofmann-Wellenhof, B., Lichtenegger, B., and Collins, J. *Global Positioning System*. New York: Springer-Verlag Wien, 2001.

[6] Kaplan, E. D., and Hegarty, C. J. *Understanding GPS: Principles and Applications* (2nd ed.). 2006.

[7] Yoon, D., Kee, C., Seo, J., and Park, B. Position accuracy improvement by implementing the DGNSS-CP algorithm in smartphones. PubMed, 2016, DOI: 10.3390/s16060910.

[8] Aghaei, M., Dolara, A., Leva, S., and Grimaccia, F. Image resolution and defects detection in PV inspection by unmanned technologies. In *Proceedings of the 2016 IEEE Power and Energy Society General Meeting* (PESGM), Jul. 2016, 1–5.

[9] Kurtz, S., Packard, C., Jahn, U., Berger, K., and Kato, K. Performance and reliability of photovoltaic systems subtask 3.2: Review of failures of photovoltaic modules. International Energy Agency. [Online]. Available: http://iea-pvps.org/index.php?id=275&eID=dam_frontend_push&docID=2064.

[10] Mastny, P., Radil, L., and Mastna, Z. Possibilities of PV panels defects identification and determination of its effect on the economy of photovoltaic power plants operation. In *Proceedings of the 2nd International Conference on Mathematical Models for Engineering Science*, Stevens Point, WI, 2011, 233–238.

[11] Brunelli, R. *Template Matching Techniques in Computer Vision: Theory and Practice*. Wiley Publishing, 2009.

[12] Zelinsky, A. Learning OpenCV—Computer vision with the OpenCV library (Bradski, G.R. et al., 2008). *IEEE Robotics Automation Magazine*, Vol. 16, 3 (Sep. 2009), 100–100.

[13] Mahmood, A., and Khan, S. Correlation-coefficient-based fast template matching through partial elimination. *IEEE Transactions on Image Processing*, Vol. 21, 4 (Apr. 2012), 2099–2108.

CALL FOR PROPOSALS

2022 IEEE Radar Conference (RadarConf22)

The Radar Systems Panel (RSP) of the IEEE Aerospace & Electronic Systems Society welcomes proposals from prospective organizers to host the *2022 IEEE Radar Conference*. This conference series, originally initiated in 1984 as the *US National Radar Conference*, has grown to have an internationally diverse attendance and a reputation for the highest quality. The RadarConf series is the premier forum for the technological advancement of the field of radar including theoretical and experimental results for a diverse array of civil, scientific, and defense applications. Topics include, but are not limited to:

- Radar Phenomenology (e.g. scattering, phenomenology)
- Components (e.g. digital RF, photonics, mm-wave)
- Signal Processing (e.g. detection, tracking, classification, STAP)
- Synthetic Aperture (e.g. FOPEN, RF tomography, remote sensing)
- Antennas (e.g. phased arrays, conformal)
- Civil/Scientific Applications (e.g. automotive, weather, planetary mapping, navigation)
- Waveform Diversity (e.g. MIMO, pulse agility, bistatic/multistatic, noise radar)
- Emerging Technologies (e.g. Terahertz sensing, meta-materials)

Prior to submitting a proposal, AESS members interested in hosting RadarConf22 should send a notice of intent via email to Prof. Shannon Blunt. As part of a formal proposal, interested parties will be asked to demonstrate sufficient anticipated support from radar industry, facilities amenable for hosting the conference, and a financial plan according to IEEE requirements. To enable discussion at the RSP meeting to be held at the 2019 Radar Conference in Boston (in April), a formal notice of intent is requested prior to 1 January 2019 and a written proposal by 15 March 2019. Proposers will subsequently be asked to present their proposal at the RSP meeting.

Prof. Shannon Blunt
Chair, RSP Conferences Committee
sdblunt@ittc.ku.edu